PNAS RESEARCH ARTICLE | BIOPHYSICS AND COMPUTATIONAL BIOLOGY OPEN ACCESS

Unbalanced bidirectional radial stiffness gradients within the organ of Corti promoted by TRIOBP

Hesam Babahosseini[a,1], Inna A. Belyantseva[b,1], Rizwan Yousaf[b], Risa Tona[b], Shadan Hadi[c], Sayaka Inagaki[b], Elizabeth Wilson[b], Shin-ichiro Kitajiri[d], Gregory I. Frolenkov[c], Thomas B. Friedman[b], and Alexander X. Cartagena-Rivera[a,2]

Edited by Andrei Kozlov, Imperial College London, London, United Kingdom; received August 19, 2021; accepted May 12, 2022 by Editorial Board Member Jeremy Nathans

Hearing depends on intricate morphologies and mechanical properties of diverse inner ear cell types. The individual contributions of various inner ear cell types into mechanical properties of the organ of Corti and the mechanisms of their integration are yet largely unknown. Using sub-100-nm spatial resolution atomic force microscopy (AFM), we mapped the Young's modulus (stiffness) of the apical surface of the different cells of the freshly dissected P5–P6 cochlear epithelium from wild-type and mice lacking either Trio and F-actin binding protein (TRIOBP) isoforms 4 and 5 or isoform 5 only. Variants of *TRIOBP* are associated with deafness in human and in *Triobp* mutant mouse models. Remarkably, nanoscale AFM mapping revealed unrecognized bidirectional radial stiffness gradients of different magnitudes and opposite orientations between rows of wild-type supporting cells and sensory hair cells. Moreover, the observed bidirectional radial stiffness gradients are unbalanced, with sensory cells being stiffer overall compared to neighboring supporting cells. Deafness-associated TRIOBP deficiencies significantly disrupted the magnitude and orientation of these bidirectional radial stiffness gradients. In addition, serial sectioning with focused ion beam and backscatter scanning electron microscopy shows that a TRIOBP deficiency results in ultrastructural changes of supporting cell apical phalangeal microfilaments and bundled cortical F-actin of hair cell cuticular plates, correlating with messenger RNA and protein expression levels and AFM stiffness measurements that exposed a softening of the apical surface of the sensory epithelium in mutant mice. Altogether, this additional complexity in the mechanical properties of the sensory epithelium is hypothesized to be an essential contributor to frequency selectivity and sensitivity of mammalian hearing.

biophysics | mechanobiology | hearing mechanics | atomic force microscopy | actin cytoskeleton

Significance

Current understanding of cochlear mechanics assumes that stiffness of the cochlear partition varies only longitudinally along the cochlea. This work examines the stiffness of inner ear epithelium in individual cell types at the nanoscale level. We revealed unrecognized radial stiffness gradients of different magnitudes and opposite orientations within the epithelium. Remarkably, the observed bidirectional stiffness gradients are unbalanced between supporting and sensory cells. Deficiencies in deafness-associated Trio and F-actin binding protein (TRIOBP) caused diverse cytoskeletal ultrastructural remodeling in supporting and sensory cells and significantly diminishes the bidirectional radial stiffness gradients. These results demonstrate the complexity of the mechanical properties within the sensory epithelium and point to a hitherto unrecognized role of these gradients in sensitivity and frequency selectivity of hearing.

In the inner ear, the sensory epithelium of the organ of Corti detects and amplifies sound vibrations with exquisite sensitivity. The specialized cell types of the organ of Corti have intricate morphologies and together build an ultrasensitive electrochemical and mechanical machine. Mechanosensitive hair cells are flanked by supporting cells providing resistance to mechanical deformations from sound stimulation (1) and yet allow propagation of sound waves. Sensory cells in the cochlea are organized in rows along the cochlear spiral with one row of inner hair cells (IHCs) and three rows of outer hair cells (OHCs) (Fig. 1). The sensory IHCs transduce sound and convey auditory information directly to the brain's auditory nuclei, while OHCs amplify weak sound-evoked vibrations (2). Supporting cells in the organ of Corti include inner pillar cells (IPCs), outer pillar cells (OPCs), and three rows of Deiters' cells (DCs) (Fig. 1). The apical surfaces of IPCs are located between the IHCs and OHCs, while OPCs extend their apical surfaces between the first row of OHCs and make a contact with the second row of OHCs. The apical plates and processes of DCs separate the other two rows of OHCs (Fig. 1). The apical plates of DCs and OPCs are the main constituents of the reticular lamina (Fig. 1) that extends from the heads of OPCs to the Hensen's cells and immobilizes the OHC cuticular plates. Together with OHCs, these supporting cells are interconnected by tight junctions that provide boundaries between the endolymph and perilymph compartments and prevent mixing of these two fluids that have very different ionic compositions (3). The reticular lamina also provides structural support and facilitates the exceptional sensitivity of hair cells required for normal sound transduction (4).

To transduce sound, each hair cell has a mechanoreceptive hair bundle with stereocilia rows of increasing height organized in a staircase arrangement (5). In response to sound, a stereocilia bundle is deflected a few tens to 100 nm, which opens tension-gated mechanoelectrical transduction ion channels located at the tips of shorter row stereocilia (6). Each stereocilium has a paracrystalline filamentous actin (F-actin) core consisting of hundreds of unidirectionally oriented, bundled, and cross-linked actin

Author contributions: I.A.B., T.B.F., and A.X.C.-R. designed research; H.B., I.A.B., R.Y., R.T., S.H., S.I., G.I.F., and A.X.C.-R. performed research; I.A.B., R.Y., E.W., S.K., and A.X.C.-R. contributed new reagents/analytic tools; H.B., I.A.B., R.Y., R.T., S.H., G.I.F., and A.X.C.-R. analyzed data; H.B., I.A.B., T.B.F., and A.X.C.-R. wrote the paper; and A.X.C.-R. supervised research work.

The authors declare no competing interest.

This article is a PNAS Direct Submission. A.K. is a guest editor invited by the Editorial Board.

[1]H.B. and I.A.B. contributed equally to this work.

[2]To whom correspondence may be addressed. Email: cartagenariveax@nih.gov.

This article contains supporting information online at http://www.pnas.org/lookup/suppl/doi:10.1073/pnas.2115190119/-/DCSupplemental.

Published June 23, 2022.

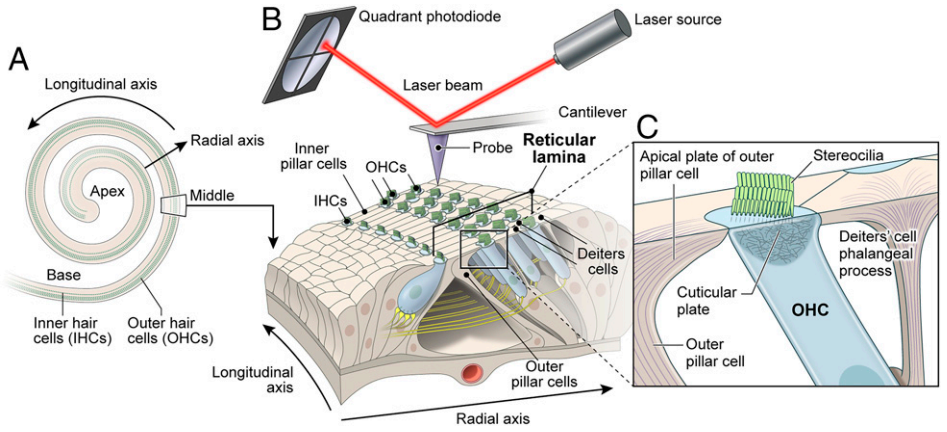

Fig. 1. Schematic of the organ of Corti sensory epithelium, hair cells, supporting cells cellular structures, and the experimental system for PFT-AFM measurements. (*A*) The schematic illustrates the coiled shape of the inner ear auditory sensory epithelium and the orientations of the longitudinal and radial axes. (*B*) The PFT-AFM experimental setup that was used to measure nanoscale stiffness of the organ of Corti reticular lamina of sensory epithelium segment including three rows of OHCs and the supporting cells (IPCs, OPCs, and three rows of DCs). (*C*) Close-up view of the longitudinal cross-section through the OHC and surrounding supporting cells showing the F-actin–based cuticular plate, stereocilia bundle of OHC, OPC apical plate, and DC's phalangeal process.

filaments (5). Adjacent stereocilia in a bundle are interconnected by a variety of extracellular links (5). Each stereocilium is anchored into the apical hair cell body by an F-actin–based rootlet that is embedded in the cuticular plate, a rigid filamentous actin cytoskeletal structure located below the apical plasma membrane of a hair cell (7) (Fig. 1). Stereocilia are rigid structures. When deflected by sound waves, all stereocilia within a hair bundle bend at their insertion points in the hair cell (8). A rootlet is embedded in the F-actin stereocilium core from approximately one-third to one-half the stereocilium length and about the same distance in the opposite direction into the cuticular plate where each rootlet is anchored (7).

The elaborate F-actin cytoskeleton of hair cells requires many actin-bundling proteins. One of them that is essential for stereocilia rootlet development and function is TRIOBP (Trio and F-actin binding protein), which is also required as an important component of the apical cytoskeleton of adjacent supporting cells (9, 10). There are three classes of alternative splice messenger RNA (mRNA) isoforms transcribed from the mouse *Triobp* and human *TRIOBP* genes encoding the proteins TRIOBP-1, TRIOBP-4, and TRIOBP-5 (9). Mouse *Triobp-4* mRNA is transcribed from the first eight exons of the *Triobp* gene and encodes the 107-kDa TRIOBP-4 protein that has unusual repeated motifs that bind and tightly bundle actin filaments (11). TRIOBP-5 is a 218-kDa protein (11) which includes all of the amino acid sequence of TRIOBP-4 at its N terminus while the remainder of TRIOBP-5 has five predicted coiled-coil domains and a pleckstrin homology (PH) domain (9, 10, 12). TRIOBP-1 is the smallest of the three isoforms (72 kDa, also named Tara, Trio-associated repeat on actin) (12). *Triobp-1* mRNA has a unique first exon with its own transcription start site located between exons 12 and 13 of the *Triobp* gene, while the rest of the *Triobp-1* mRNA is identical to exons 13 through 25 of *Triobp-5* mRNA. TRIOBP-1 protein binds and stabilizes F-actin structures (12–15), shows a broad expression pattern throughout the body, and, at least in the mouse, is required for embryonic viability. However, TRIOBP-4 and TRIOBP-5 are only necessary for normal hearing (9, 10, 16–21). Most of the recessive variants of human *TRIOBP* are associated with profound deafness DFNB28 and are located in the large exon 6, orthologous to mouse exon 8, and thus they mutate simultaneously both TRIOBP-4 and TRIOBP-5 (TRIOBP-4/5) proteins (16, 17). To date, variants that damage only the TRIOBP-5 isoform are associated in humans with moderate to severe deafness or age-related hearing loss (18–20).

In mouse inner ear hair cells, TRIOBP is mainly localized to stereocilia rootlets (9, 10). Deficiency of both TRIOBP-4 and TRIOBP-5 (TRIOBP-4/5) results in a total absence of rootlets. However, a deficiency only of TRIOBP-5 results in dysmorphic stereocilia rootlets and a progressive loss of hearing (9, 10, 22). TRIOBP is also expressed in supporting cells of the sensory epithelium and is localized in the apical processes of IPCs, OPCs, and three rows of DCs. We recently reported a critical role of the TRIOBP-5 protein in supporting cell mechanics (10). Exactly how the overall micromechanics of the cochlear reticular lamina depends on the functions of different TRIOBP isoforms is understudied. Understanding the composite of TRIOBP functions in cochlear mechanics requires a comprehensive investigation of the mechanical properties of the different individual cell types in the inner ear at nanoscale resolution. We hypothesize that the highly divergent cell types in the organ of Corti show multidimensional but interconnected mechanical relationships.

The mechanical resistance of individual cells interacting in a live organ of Corti is critical for sound wave propagation and transduction. In previous studies, the cochlear micromechanical properties at the cellular level have been measured in spatially restricted areas, such as the stereocilia bundles, using glass micropipettes (23, 24), fluid jets (25), or standard atomic force microscopes (26). Quasi-static atomic force microscopy (AFM) was also utilized to characterize the surface Young's modulus of OHCs and supporting PCs in the mouse cochlea at early ages (postnatal day [P]0 to P5) (27). Due to the low spatial resolution of these studies, the cochlear mechanical properties were not mapped. Changes in Young's modulus of the cochlear basilar membrane using PeakForce Tapping AFM (PFT-AFM) technique was reported (28). However, to date no study has systematically measured in a holistic manner at nanoscale resolution the mechanical properties of the spatially heterogenous apical surface of the cochlear sensorial reticular lamina of wild-type and mutant mice with cytoskeletal alterations of the different cells of the organ of Corti.

In this study, we used PFT-AFM to measure the axial elastic modulus of the reticular lamina including individual OHC cuticular plates, the apical surfaces of the PCs, and the apical processes of DCs (Fig. 1). We also investigated how a combined TRIOBP-4 and TRIOBP-5 deficiency, or a TRIOBP-5 deficiency alone, affects the apical stiffness of individual cells. In doing so, we identified additional functions of TRIOBP-4 and TRIOBP-5 in the modulation of the reticular lamina micromechanics in the organ of Corti. Intriguingly, we discovered previously unknown radial direction stiffness gradients of opposite orientations and magnitudes for supporting cells and hair cells. The absence of both TRIOBP isoforms significantly reduces the magnitude and affects the orientation of these radial stiffness gradients, which are essential for optimal tissue-level nanomechanics of the auditory sensory epithelium.

Results

Quantification of Triobp-4 and Triobp-5 mRNAs Expressed in Mouse Organ of Corti. TRIOBP has multiple cytoskeletal functions in different inner ear cell types. The expression of mouse TRIOBP-4 and TRIOBP-5 was examined using a LacZ cassette (*Escherichia coli* β-galactosidase) that replaced all of the sequence of mouse *Triobp* exon 8. Therefore, β-galactosidase cellular expression is a proxy for both TRIOBP-4 and TRIOBP-5 proteins because exon 8 sequence is included in both *Triobp-4* and *Triobp-5* mRNAs. Staining for β-galactosidase activity in the sensory epithelium of the inner ear (9), however, could not discriminate the *Triobp*-driven LacZ signal for *Triobp-5* from a signal of *Triobp-4* expression. Therefore, rather than a LacZ reporter, in this study we examined in situ *Triobp* mRNA expression using RNAscope probes specific for 1) both *Triobp-4 and Triobp-5* mRNAs (*Triobp-4/5*) (Fig. 2*A*, *Left and Middle*), 2) both the *Triobp-1* and *Triobp-5* mRNAs (*Triobp-1/5*) (Fig. 2*B*, *Left and Middle*), and 3) only the *Triobp*-5 mRNA (Fig. 2 *A* and *B*, *Right*). In wild-type mouse cochlea at P6, *Triobp-5* mRNA expression is prominent in OHCs and to a lesser extent in IHCs and supporting cells. A similar pattern was observed when an RNAscope probe specific for *Triobp-1/5* mRNA was utilized. In addition to the hair cell signal, there was a weaker signal in supporting cells. In contrast, an RNAscope probe specific for *Triobp-4/5* mRNAs shows a more broadly distributed signal highlighting both hair cells and supporting cells, including cells of the greater epithelial ridge (Fig. 2*A*, *Middle*). This pattern of expression of *Triobp-4/5* mRNA is consistent with the reported role of TRIOBP-4, which is necessary for stereocilia rootlet formation and the initial development of the cytoskeletal components of supporting cells required for their structural role in the reticular lamina (9). The pattern of TRIOBP-5 mRNA expression at P6 is consistent with the reported conclusion that this isoform plays major roles in the maturation of stereocilia rootlet architecture and in the development of cytoskeletal structures of the supporting cells, which becomes critically important after the onset of hearing at P12 (9, 10).

Quantification of expression levels of the three different *Triobp* isoforms in the inner ear of P6 $Triobp^{\Delta Ex9\text{-}10}$ mutant mice, deficient only for the TRIOBP-5 isoform, was also evaluated using droplet digital PCR (ddPCR). In heterozygous $Triobp^{\Delta Ex9\text{-}10/+}$ mice, there was a reduction of *Triobp-5* expression level to approximately one-half of the wild type. These data indicate that there is no increase in mRNA expression from the remaining single wild-type copy of the *Triobp* gene to compensate for the loss of one allele in heterozygotes. As expected, no expression of *Triobp-5* mRNA was detected in the homozygous $Triobp^{\Delta Ex9\text{-}10/\Delta Ex9\text{-}10}$ mouse (*SI Appendix*, Fig. S1*B*). In addition, no significant difference in the expression level of either *Triobp-1 or Triobp-4* mRNAs was observed in the homozygous $Triobp^{\Delta Ex9\text{-}10/\Delta Ex9\text{-}10}$ mice, indicating that the $Triobp^{\Delta Ex9\text{-}10}$ allele does not induce an up-regulation or down-regulation of the *Triobp-1* or *Triobp-4* mRNAs (*SI Appendix*, Fig. S1*B*) and by inference their protein levels.

Localization of TRIOBP-1, TRIOBP-4, and TRIOBP-5 in the Wild-Type and TRIOBP-5–Deficient Mouse Organ of Corti. We previously showed the distribution of TRIOBP-4 and TRIOBP-5 in hair cell cuticular plates, stereocilia rootlets, and in the apical projections of the DCs of wild-type and $Triobp^{\Delta Ex9\text{-}10/\Delta Ex9\text{-}10}$ mice (10). However, localization of TRIOBP-1 was not previously investigated for lack of a TRIOBP-1–specific antibody since most of the sequence of TRIOBP-1 is identical to the C-terminal part of TRIOBP-5. We recently validated an anti-TARA antibody using our $Triobp^{\Delta Ex9\text{-}10/\Delta Ex9\text{-}10}$ mice (29) and showed that the antibody signal in stereocilia rootlets solely represents the TRIOBP-5 isoform. Consequently, to investigate the correlation of our expression data of *Triobp-1*, *Triobp-4*, and *Triobp-5* mRNAs with the corresponding protein isoform localizations, we used TRIOBP4/5-specific and anti-TARA antibodies in $Triobp^{+/+}$ and $Triobp^{\Delta Ex9\text{-}10/\Delta Ex9\text{-}10}$ mice. Since the TRIOBP-5 protein isoform is absent in $Triobp^{\Delta Ex9\text{-}10/\Delta Ex9\text{-}10}$ mice, we interpret the remaining signal from the anti-TARA antibody in the mutant organ of Corti as being specific to TRIOBP-1 and the remaining signal from TRIOBP-4/5 antibody as specific for TRIOBP-4. In addition, by comparing immunoreactivity of $Triobp^{\Delta Ex9\text{-}10/\Delta Ex9\text{-}10}$ mutant to the wild type, we can determine the signal corresponding to TRIOBP-5. Our immunostaining (Fig. 3) shows that both TRIOBP-4 (Fig. 3 *A* and *B*) and TRIOBP-5 (Fig. 3 *A* and *C*) are present in DC apical processes (arrows in Fig. 3 *A*–*C*, *Insets*) and hair cell stereocilia rootlets but absent from the nonsensory cells of the internal and external sulcus (Fig. 3 *A* and *B*). In contrast, TRIOBP-1 is present in the nonsensory cells of the external and internal sulcus (arrowheads in Fig. 3 *C* and *D*) and in the cell junctions between hair cells and supporting cells of the organ of Corti as well as diffusely distributed in hair cell cuticular plates (Fig. 3*D*, asterisks). We did not observe a TRIOBP-1 signal in stereocilia rootlets using the anti-TARA antibody (Fig. 3*D*, asterisks). This correlates with our previous findings that in the absence of both TRIOBP-4 and TRIOBP-5 but in the presence of TRIOBP-1 rootlets are absent (9). Also, TRIOBP-1 does not localize to the apical projections of the supporting cell (Fig. 3*D* and inset), where TRIOBP-4 and TRIOBP-5 are found (Fig. 3 *A*–*C*). Although not quantitative, these immunochemistry observations appear to support no differences in the TRIOBP-1 (Fig. 3 *C* and *D*) or TRIOBP-4 (Fig. 3 *A* and *B*) immunoreactivity in $Triobp^{\Delta Ex9\text{-}10/\Delta Ex9\text{-}10}$ mutant mice as compared to the wild-type controls, consistent with our mRNA expression data (*SI Appendix*, Fig. S1).

TRIOBP-5 Deficiency Results in Ultrastructural Defects in OHCs, OPCs, and DCs. The effects of TRIOBP deficiency on hair cell stereocilia rootlet formation and architecture are published (9, 10). However, the ultrastructural changes in the other regions of hair cells and in supporting cells have not been investigated by electron microscopy. To explore these potential changes, we used serial sectioning with focused ion beam and backscatter scanning electron microscopy imaging (FIB-SEM) that provides a lateral X–Y resolution of 2 to 3 nm and a sectioning step of 20 nm in the high-pressure frozen freeze-substituted cochlear explants. In heterozygous $Triobp^{\Delta Ex9\text{-}10/+}$ mice at P6, virtual transverse reslicing of an OHC in the registered FIB-SEM stack revealed regular cortical filamentous actin tangles at the top of the cuticular plate (Fig. 4*A*, yellow arrows). Wild-type $Triobp^{+/+}$ mice at P7 revealed similar regular actin "tangles" at the top of the cuticular plate (*SI Appendix*, Fig. S3*B*). However, these regular cortical actin "tangles" were not observed in homozygous TRIOBP-5–deficient littermates (Fig. 4*A*). The disruption of cuticular plate F-actin in $Triobp^{\Delta Ex9\text{-}10/\Delta Ex9\text{-}10}$ OHCs represents either a direct effect of TRIOBP-5 deficiency or F-actin rearrangement associated with the abnormalities of stereocilia rootlets in these mice (10).

Besides hair cell rootlets and cuticular plates, TRIOBP is also localized to the apical phalangeal projections of IPCs, OPCs, and DCs (Figs. 2, 3, and 4*B*). The apical phalangeal microtubular projections are located deeper, at the level of the bottom edges of the hair cell cuticular plates. Transverse Z-projection of the 400-nm-thick

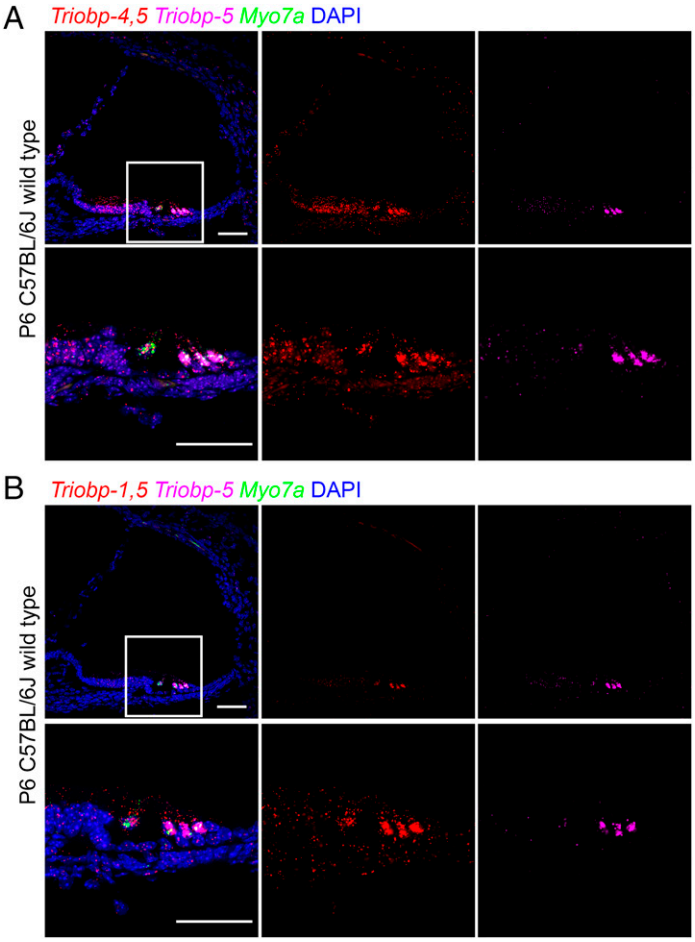

Fig. 2. In situ hybridization using RNAscope probe in P6 wild-type mouse cochlea. (*A*) Expression of *Triobp-4 and Triobp-5* mRNAs (*Triobp-4/5*) (red, Probe-Mm-Triobp-O1), *Triobp-5* only mRNA (magenta, Probe-Mm-Triobp-O2-C3), and *Myo7a* mRNA (green, Probe-Mm-Myo7a-C2). *Triobp-4/5* mRNA (red) is expressed in IHCs and OHCs and supporting cells, whereas mRNA of *Triobp-5* alone is expressed mainly in OHCs. (*B*) Expression of both *Triobp-1 and Triobp-5* mRNA (*Triobp-1/5*) (red, Probe-Mm-Triobp-O3), *Triobp-5* only mRNA (magenta, Probe-Mm-Triobp-O2-C3), and *Myo7a* mRNA (green, Probe-Mm-Myo7a-C2). *Triobp-1/5* mRNA was detected mainly in hair cells. (Scale bars: 50 μm.)

FIB-SEM volume at this level revealed distinct filament/microtubule structures in normal hearing $Triobp^{\Delta Ex9\text{-}10/+}$ OPCs (Fig. 4*C*, arrow) and dense actin patches in $Triobp^{\Delta Ex9\text{-}10/+}$ DCs (Fig. 4*C*, arrowhead). Likewise, wild-type $Triobp^{+/+}$ mice at P7 revealed similar microfilaments/microtubules structures (*SI Appendix*, Fig. S3 *A* and *D*). These structures were either disrupted or barely visible in homozygous deaf $Triobp^{\Delta Ex9\text{-}10/\Delta Ex9\text{-}10}$ littermates (Fig. 4*C*). It is worth mentioning that, besides microtubules (3), the apical projections of IPCs, OPCs, and DCs also contain actin filaments that can be revealed by β-actin immunolabeling (Fig. 4*D*). Sagittal reslicing of FIB-SEM volume parallel to the filament/microtubule structures in OPCs showed that they are present in wild-type $Triobp^{+/+}$, $Triobp^{\Delta Ex9\text{-}10/+}$, and $Triobp^{\Delta Ex9\text{-}10/\Delta Ex9\text{-}10}$ mice (Fig. 4*E*; see also *SI Appendix*, Fig. S3*C*); however, their density and regularity are impaired in mutant $Triobp^{\Delta Ex9\text{-}10/\Delta Ex9\text{-}10}$ OPCs (Fig. 4*E*, *Insets*). Thus, TRIOBP-5 deficiency results in ultrastructural defects in OHCs, PCs, and DCs, which are the three major types of cells that form reticular lamina of the organ of Corti.

Absence of TRIOBP-5 Softens Apical Surfaces of Supporting and Hair Cells and Stereocilia Rootlets. To investigate the role that TRIOBP isoforms exert on cochlear cell cytoskeletons architecture and on the mechanical resistance of cochlear sensory epithelia, we measured the Young's elastic modulus (E, stiffness) of the reticular lamina of wild-type and *Triobp* mutant mice using PFT-AFM. Both topography and mechanical mapping were obtained simultaneously by gently indenting the apical surface (<500 nm) of living mouse organ of Corti explants at postnatal ages P5 to P6 (P5-P6) under physiologically relevant conditions. PFT-AFM nanomechanical mapping was conducted in the middle turn of the mouse organ of Corti along the radial axis of freshly dissected sensory epithelial explants.

The Young's modulus of the localized nano-indented cells within the reticular lamina was calculated. Nanoscale stiffness maps were generated using live P5-P6 organ of Corti of $Triobp^{+/+}$ (wild type), heterozygous $Triobp^{\Delta Ex9\text{-}10/+}$, and homozygous mutant $Triobp^{\Delta Ex9\text{-}10/\Delta Ex9\text{-}10}$ littermates (Fig. 5*A* and *SI Appendix*, Fig. S4). On the apical surfaces of PCs and DCs, localized stiffnesses of the reticular lamina of mutant $Triobp^{\Delta Ex9\text{-}10/\Delta Ex9\text{-}10}$ mice were significantly reduced ($P < 0.0001$) compared with that of normal-hearing $Triobp^{+/+}$ littermates (Fig. 5*B* and *SI Appendix*, Table S1). Thus, an absence of TRIOBP-5 protein in the organ of Corti reticular lamina significantly diminished the apical stiffness of supporting cells. Unexpectedly, we observed that the local stiffness at the apical surfaces of normal-hearing heterozygous $Triobp^{\Delta Ex9\text{-}10/+}$ mice is also significantly reduced to an intermediate level between wild-type $Triobp^{+/+}$ and $Triobp^{\Delta Ex9\text{-}10/\Delta Ex9\text{-}10}$ for PCs ($P < 0.01$) and DCs ($P < 0.0001$), arguing for a wild-type gene dose-dependent influence of TRIOBP-5 on the apical stiffness of supporting cells. Our quantitative ddPCR data described above indicate that heterozygous $Triobp^{\Delta Ex9\text{-}10/+}$ mice have reduced *Triobp5* mRNA expression that is approximately one-half that of the wild-type level (*SI Appendix*, Fig. S1*B*). However, the reduction in stiffness of the reticular lamina in young heterozygote mice does not significantly harm the hearing ability later on, as indicated by auditory brainstem response analyses at P14 (10). Whether or not a heterozygous carrier of a recessive pathogenic variant of *TRIOBP*/*Triobp* is more susceptible to age-related hearing loss or

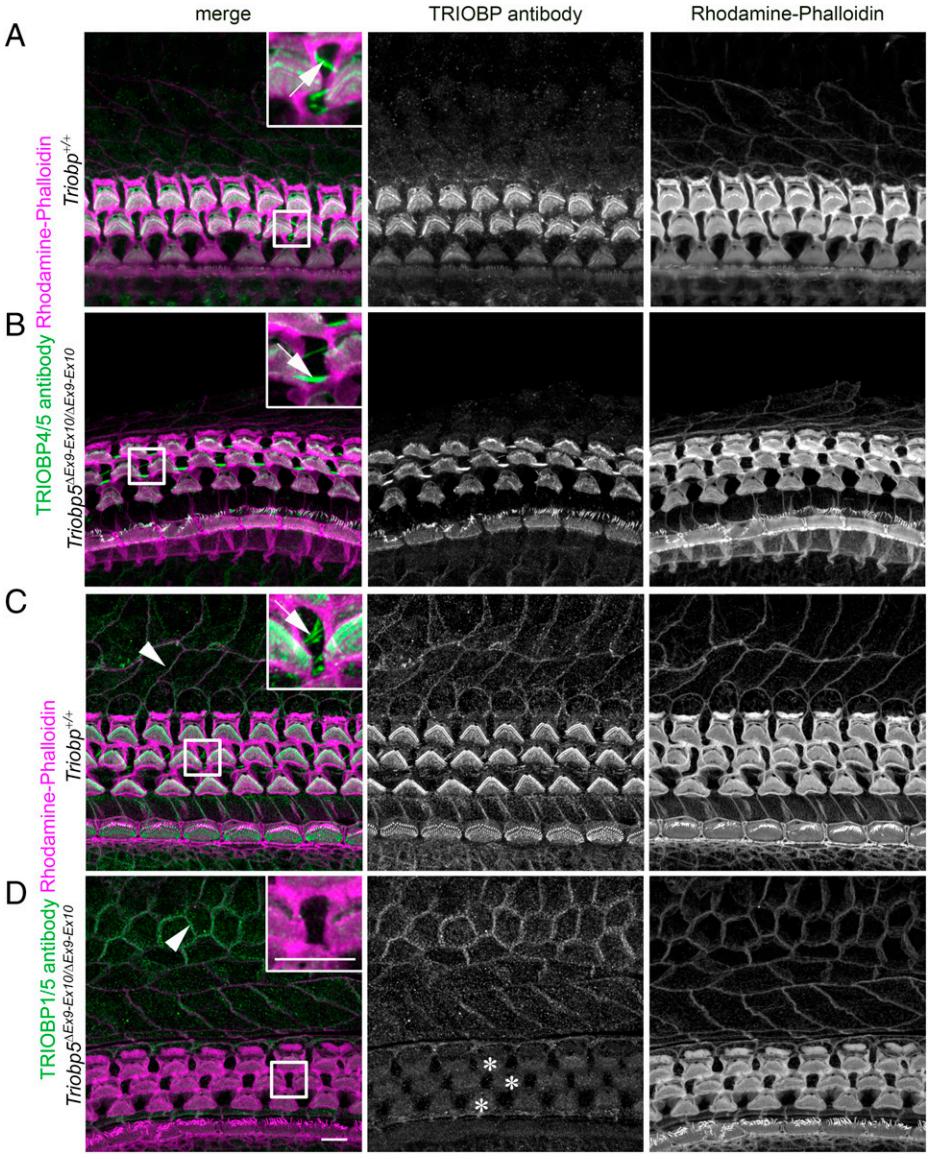

Fig. 3. Localization of TRIOBP-1 and TRIOBP-4 proteins are unaffected by the absence of TRIOBP-5 in *Triobp*$^{\Delta Ex9\text{-}10/\Delta Ex9\text{-}10}$ mouse organ of Corti. (*A*) P8 wild-type mouse organ of Corti stained with TRIOBP-4/5 antibody. (*Inset*) An enlarged image of the area outlined by the square shape depicting TRIOBP-4/5 immunoreactivity (green) present in stereocilia rootlets and the cuticular plate of OHCs (*Inset*) and in microfilaments of DCs (arrow in the *Inset*). (*B*) TRIOBP-4 (green) but not TRIOBP-5 is detected and localized to the stereocilia rootlets of OHCs (*Inset*) and microfilaments of DCs (arrow in the *Inset*) in P8 TRIOBP-5–deficient littermate mouse. (*C*) P8 wild-type mouse organ of Corti stained with anti-TARA antibody developed against the C-terminal 374 residues present in both TRIOBP-5 and TRIOBP-1. (*Inset*) Enlarged image of the area outlined by the square depicting TRIOBP-1/5 immunoreactivity (green) present in stereocilia rootlets and the cuticular plates of OHCs (*Inset*) and in microfilaments of DCs (arrow in the *Inset*). (*D*) Immunostaining of *Triobp*$^{\Delta Ex9\text{-}10/\Delta Ex9\text{-}10}$ mouse organ of Corti using TRIOBP-1/5 antibody reveals that stereocilia rootlet and DC signals observed in wild-type mouse (*C*) correspond to TRIOBP-5, while nonsensory cell junction signals of the external and internal sulcus cells represent TRIOBP-1 (arrowheads in *C* and *D*). TRIOBP-1 was detected also at the junctions of the hair cells and supporting cells of the organ of Corti and diffusely distributed in the cuticular plates of OHCs (asterisks). (Scale bars in *D* and *D*, *Inset*: 5 μm [applies to all panels and *Insets*].)

the organ of Corti is at greater risk of damage from loud noise is now an important question to explore. Relevant to this issue, in a large human cohort a genome-wide association study identified a missense variant of *TRIOBP* that affects only the *TRIOBP*-5 isoform and is associated with age-related hearing loss (18).

Notably, TRIOBP-5 is expressed in sensory epithelium supporting cells and localized to cytoskeletal filamentous structures within the DCs apical processes and apical surfaces of IPCs and OPCs (10). In *Triobp*$^{\Delta Ex9\text{-}10/\Delta Ex9\text{-}10}$ mice, a TRIOBP-5–specific antibody signal is absent from supporting cells (10). Therefore, a reduction in the apical stiffness of supporting cells likely results from an alteration of these developing cytoskeletal filamentous structures in supporting cells of mutant *Triobp*$^{\Delta Ex9\text{-}10/\Delta Ex9\text{-}10}$ mice, which could later affect sound-induced intracochlear vibrations and hearing function (27, 30, 31).

In addition, the local stiffnesses of the cuticular plates in OHCs of mutant *Triobp*$^{\Delta Ex9\text{-}10/\Delta Ex9\text{-}10}$ mice are significantly reduced (varying from $P < 0.001$ to 0.1) as compared with wild-type *Triobp*$^{+/+}$ (Fig. 5*C* and *SI Appendix*, Table S1). Interestingly, similar to supporting cell mechanical behavior, we observed that the local stiffness of OHCs cuticular plates in normal-hearing heterozygous *Triobp*$^{\Delta Ex9\text{-}10/+}$ mice is also reduced compared to wild-type *Triobp*$^{+/+}$ (varying from $P < 0.01$ to 0.1). ddPCR assays confirmed a ∼60% reduction in TRIOBP-5 mRNA expression in heterozygous *Triobp*$^{\Delta Ex9\text{-}10/+}$ OHCs compared to wild-type during postnatal development at P6 (*SI Appendix*, Fig. S1*B*). Thus, TRIOBP-5 deficiency in the reticular lamina of the organ of Corti is associated with a decrease in apical stiffness of supporting cells and hair cell cuticular plates.

Next, we investigated the role of TRIOBP-5 in the pivotal stiffness of stereocilia within OHC bundles using PFT-AFM performing stereocilia nano-deflections in the excitatory (positive) direction at physiologically relevant deflection magnitudes of <200 nm (32). For OHC bundle stiffness, the local effective stiffness of mutant *Triobp*$^{\Delta Ex9\text{-}10/\Delta Ex9\text{-}10}$ mice deficient for *TRIOBP-5* is significantly reduced as compared with the wild-type *Triobp*$^{+/+}$ ($P < 0.01$) (Fig. 5*D* and *SI Appendix*, Table S1). Thus, TRIOBP-5 deficiency in the organ of Corti is sufficient to cause a change in the effective pivotal stiffness of stereocilia bundles. These observations agree with our previous results using fluid-jet deflection of the stereocilia bundle (10). Deflections of the mutant *Triobp*$^{\Delta Ex9\text{-}10/\Delta Ex9\text{-}10}$ mouse hair bundles under the fluid-jet pressure were increased more than that of *Triobp*$^{+/+}$ hair bundles at the same low stimulus intensities of <200 nm (10). Thus, with similar low stimulus intensities, the fluid-jet and PFT-AFM techniques both showed an increase in

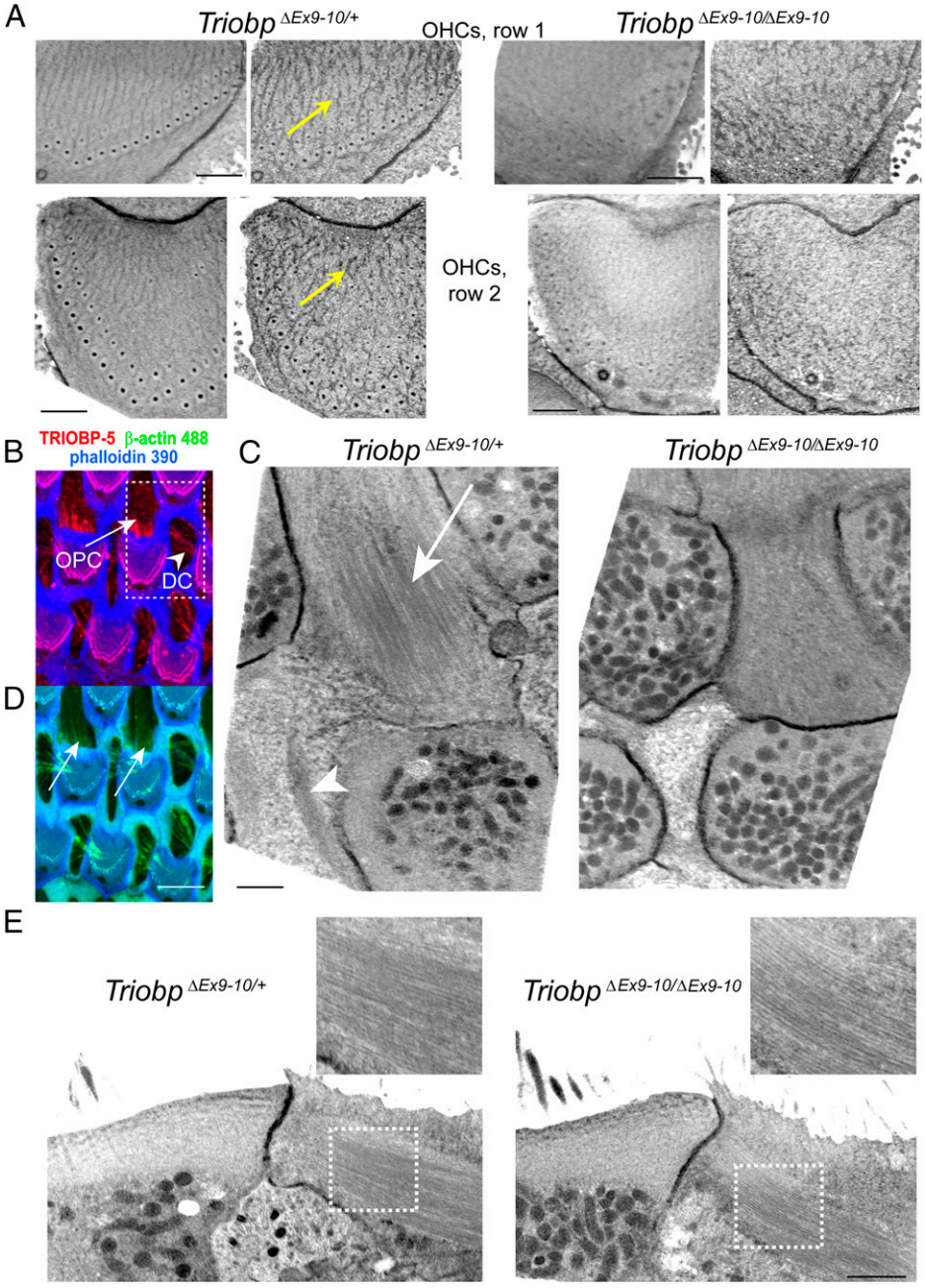

Fig. 4. Ultrastructural effects of TRIOBP-5 deficiency. (*A*) Regular cortical actin "tangles" at the upper surfaces of the OHC cuticular plates in P6 *Triobp*$^{\Delta Ex9\text{-}10/+}$ mice (*Left*, yellow arrows) and their disruption in *Triobp*$^{\Delta Ex9\text{-}10/\Delta Ex9\text{-}10}$ mice (*Right*). Similar regular actin "tangles" at the top of the OHC cuticular plate were observed in wild-type *Triobp*$^{+/+}$ mice (*SI Appendix*, Fig. S3*B*). Actin filaments were stabilized with tannic acid during fixation before staining with uranyl acetate in the freeze-substitution step (see *Materials and Methods*). Upper images illustrate first row OHCs while bottom images illustrate second row OHCs. Each cuticular plate is shown first as a median Z-projection of a 400-nm-thick FIB-SEM volume and then as a single representative FIB-SEM section. The data are representative of five *Triobp*$^{\Delta Ex9\text{-}10/+}$ OHCs and eight *Triobp*$^{\Delta Ex9\text{-}10/\Delta Ex9\text{-}10}$ OHCs. (*B*) Maximum intensity projection view of the Z-stack volume through the hair cell cuticular plates of wild-type *Triobp*$^{+/+}$ mice showing TRIOBP-5 immunofluorescence (red) and phalloidin 390 labeling of F-actin (blue) in the OHCs cuticular plate and in the OPC and DC microfilaments. (*C*) Median Z-projections of a 400-nm-thick FIB-SEM volume at the level of the bottom of the OHC cuticular plates, which show microfilaments/microtubules in OPCs (arrow) and actin patches in DCs (arrowhead) in P6 *Triobp*$^{\Delta Ex9\text{-}10/+}$ mice (*Left*) and their disruption in *Triobp*$^{\Delta Ex9\text{-}10/\Delta Ex9\text{-}10}$ mice (*Right*). Similar regular microfilaments/microtubules structures in OPCs were observed in wild-type *Triobp*$^{+/+}$ mice (*SI Appendix*, Fig. S3*D*). The data are representative of two *Triobp*$^{\Delta Ex9\text{-}10/+}$ and two *Triobp*$^{\Delta Ex9\text{-}10/\Delta Ex9\text{-}10}$ OPCs and two *Triobp*$^{\Delta Ex9\text{-}10/+}$ and three *Triobp*$^{\Delta Ex9\text{-}10/\Delta Ex9\text{-}10}$ DCs. (*D*) Fluorescent β-actin labeling (green) could be revealed in wild-type *Triobp*$^{+/+}$ mice OPCs (arrows) and in DCs in a maximum intensity projection view shown in *B*. (*E*) Lateral views of microfilaments/microtubules shown in *C*. The *Insets* show a smaller density of these structures in *Triobp*$^{\Delta Ex9\text{-}10/\Delta Ex9\text{-}10}$ OPCs. (Scale bars: 1 μm in *A*, *C*, and *E*; 5 μm in *D*.)

pivotal flexibility of stereocilia bundles of TRIOBP-5 isoform-specific knockout mice as compared to the wild-type *Triobp*$^{+/+}$ mouse.

Absence of TRIOBP-4 and TRIOBP-5 Together Further Reduces Stiffness of the Reticular Lamina and Hair Bundles. Using PFT-AFM, we generated topography and stiffness maps of P5-P6 live organ of Corti explants (middle turn) from wild-type *Triobp*$^{+/+}$, heterozygotes *Triobp*$^{\Delta Ex8/+}$, and homozygous mutant *Triobp*$^{\Delta Ex8/\Delta Ex8}$ littermates (Fig. 6*A* and *SI Appendix*, Fig. S5). On apical surfaces of PCs and DCs of *Triobp*$^{\Delta Ex8/\Delta Ex8}$ mice, deficient for both TRIOBP-4 and TRIOBP-5, local stiffness of the reticular lamina was significantly reduced ($P < 0.001$) as compared with *Triobp*$^{+/+}$ mice (Fig. 6*B* and *SI Appendix*, Table S2). The local stiffness of the PC and DC apical surfaces of heterozygous *Triobp*$^{\Delta Ex8/+}$ normal-hearing mice is also reduced compared to wild-type PCs ($P < 0.05$) and DCs ($P < 0.0001$). In comparison with changes reported for a TRIOBP-5 deficiency alone, the combined absence of TRIOBP-4 and TRIOBP-5 shows a greater decrease of the local axial stiffness of supporting cells within the reticular lamina. Since TRIOBP-4 and TRIOBP-5 were previously reported to localize to the cytoskeletal filamentous structures within the apical surfaces of the supporting PCs and DCs (10, 26), and taking into account our stiffness measurement data, we conclude that both TRIOBP-4 and TRIOBP-5 isoforms contribute to the mechanical resistance of supporting cells within the reticular lamina. Moreover, the local stiffness of the reticular lamina at the cuticular plates of hair cells of *Triobp*$^{\Delta Ex8/\Delta Ex8}$ mice is significantly reduced (varying from $P <$ 0.0001 to 0.05) compared with wild-type mice (Fig. 6*C* and *SI Appendix*, Table S2). The simultaneous deficiency for TRIOBP-4 and TRIOBP-5 in the organ of Corti resulted in a more profound decrease in the mechanical resilience of the cuticular plate of OHCs. This suggests that TRIOBP-4 and TRIOBP-5 are both reinforcing hair cell cuticular plates and the absence of both TRIOBP isoforms significantly soften the cuticular plate.

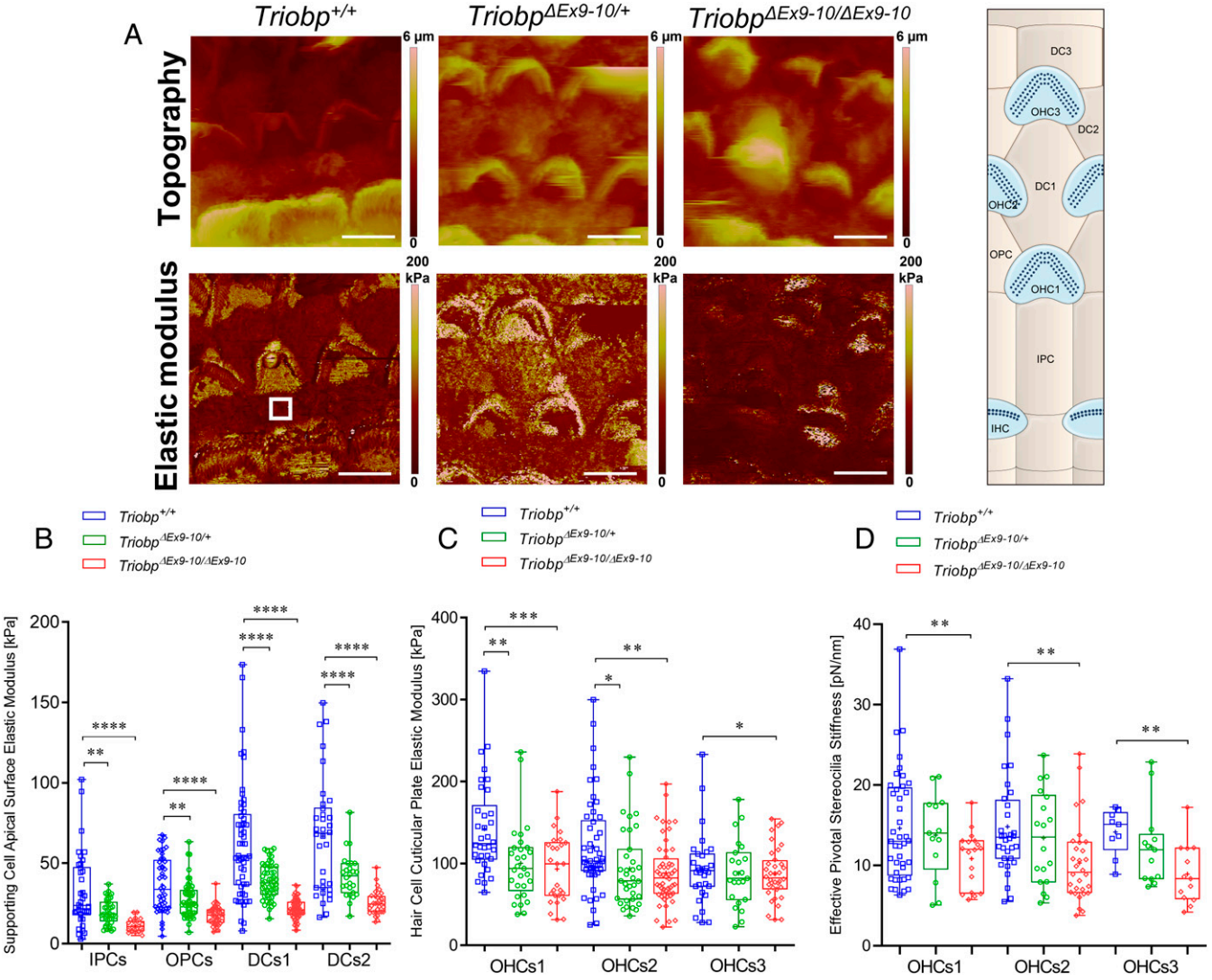

Fig. 5. TRIOBP-5 deficiency results in a significant decrease in supporting cell apical surfaces stiffness and a decrease to a lesser degree in hair cell apical surface and stereocilia bundle stiffness. (*A*) Topography and stiffness maps of the organ of Corti explants for wild-type *Triobp*$^{+/+}$, heterozygous *Triobp*$^{\Delta Ex9\text{-}10/+}$, and homozygous *Triobp*$^{\Delta Ex9\text{-}10/\Delta Ex9\text{-}10}$ mice. The schematic illustrates the locations of the apical surfaces of supporting cells phalangeal process and the hair cells cuticular plate within the reticular lamina. (*B*) E values for apical processes of IPCs, OPCs, DCs row 1 (DCs1), and DCs row 2 (DCs2) of *Triobp*$^{+/+}$, *Triobp*$^{\Delta Ex9\text{-}10/+}$, and *Triobp*$^{\Delta Ex9\text{-}10/\Delta Ex9\text{-}10}$, respectively. (*C*) E values for cuticular plates of three rows of OHCs including OHCs1, OHCs2, and OHCs3 of *Triobp*$^{+/+}$, *Triobp*$^{\Delta Ex9\text{-}10/+}$, and *Triobp*$^{\Delta Ex9\text{-}10/\Delta Ex9\text{-}10}$, respectively. The E values of the reticular lamina were measured in regions of interest (white square box in *Triobp*$^{+/+}$ Young's modulus image) overlaying the apical surface of supporting and hair cells. (*D*) Effective pivotal stereocilia stiffness values within hair bundles of three rows of OHCs. Data are represented as mean (kilopascals or piconewtons per nanometer) ± SD. Significant differences between conditions by unpaired two-tailed Student's *t* test with Welch's correction indicated as ****$P < 0.0001$, ***$P < 0.001$, **$P < 0.01$, and *$P < 0.05$. (Scale bars: 5 µm.) *SI Appendix*, Table S1 includes detailed statistical analysis.

To investigate the effects of a deficiency of both TRIOBP-4 and TRIOBP-5 on the mechanical resilience of stereocilia rootlets, we analyzed the mechanical changes of local points within the hair bundle. Local effective stiffness of the OHCs hair bundles revealed that *Triobp*$^{\Delta Ex8/\Delta Ex8}$ stereocilia are much more flexible as compared to *Triobp*$^{+/+}$ and heterozygous *Triobp*$^{\Delta Ex8/+}$ stereocilia ($P < 0.001$) (Fig. 6*D* and *SI Appendix*, Table S2). Compared to the observations of a TRIOBP-5–only deficiency, the simultaneous loss of TRIOBP-4 and TRIOBP-5 isoforms resulted in a more significant increase in the mechanical compliance of the stereocilia bundles. These results agree with an increased fragility of stereocilia from *Triobp*$^{\Delta Ex8/\Delta Ex8}$ mice that we reported previously using fluid-jet stimulations (9). At the same low stimuli intensities, the extent of the nano-deflection of the hair bundles in the TRIOBP-4/5 isoform-specific knockout mouse was significantly larger as compared with that measured in the wild type. Furthermore, our previous immunofluorescence observations revealed a restricted localization of TRIOBP-5 to the rootlet segments embedded within a hair cell cuticular plate. By comparison, TRIOBP-4 is localized along the entire length of rootlets and also diffusely distributed within the OHC cuticular plates (10). Thus, a simultaneous loss of both TRIOBP-4 and TRIOBP-5 significantly impacts resilience of the F-actin cytoskeletal structures of the hair cell cuticular plates and stereocilia bundles to a greater degree as compared to a loss of only TRIOBP-5, which in mouse results in progressive hearing loss with reduced severity compared to the profound deafness of the *Triobp* mutant mouse deficient for both TRIOBP-4 and TRIOBP-5 proteins (9, 10).

Hair Cells and Supporting Cells Have Unbalanced Radial Stiffness Gradients of Opposing Orientations. High-resolution PFT-AFM nanomechanical mapping revealed unexpected radial direction stiffness gradients in the mouse organ of Corti. The

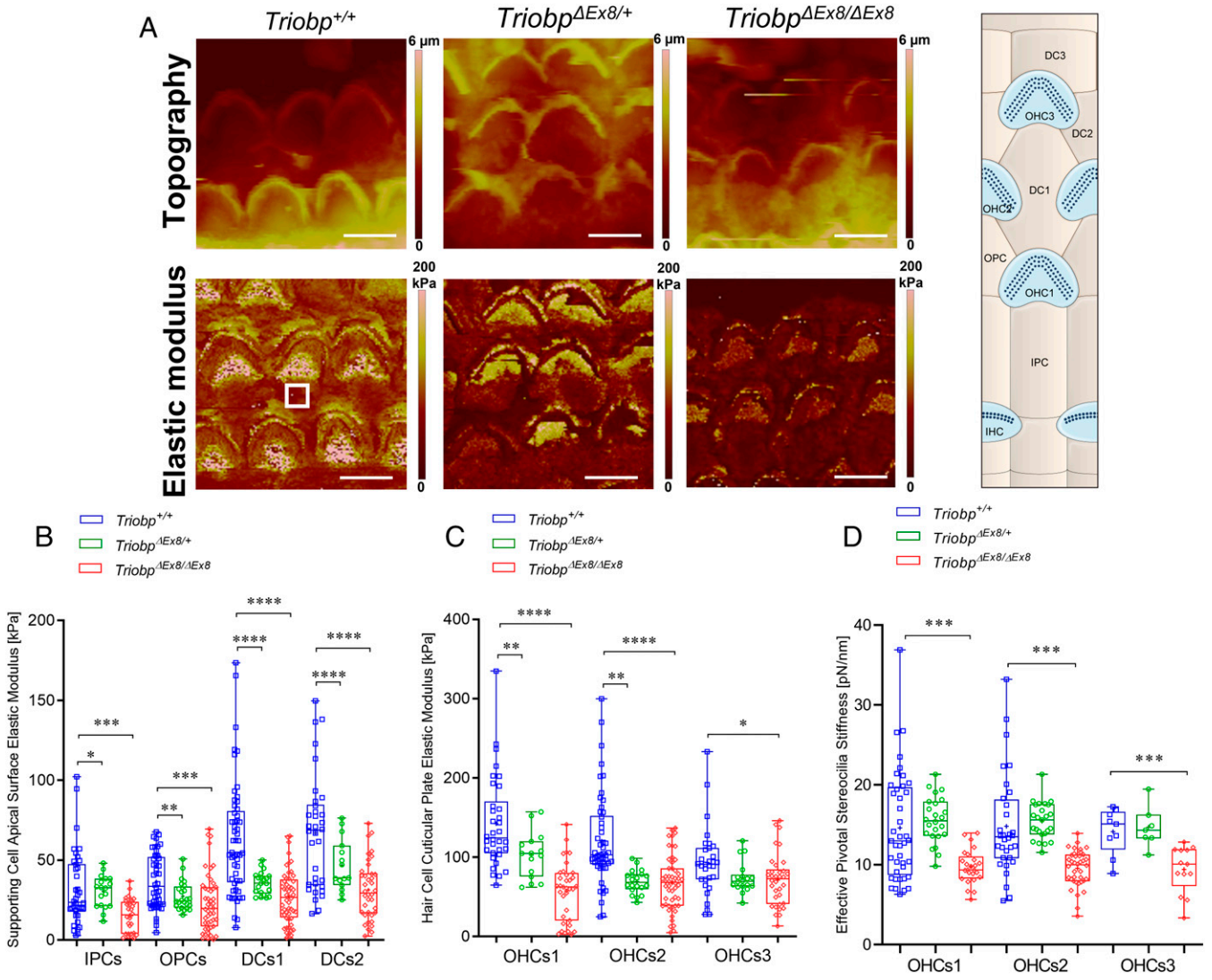

Fig. 6. Deficiency of both TRIOBP-4 and TRIOBP-5 proteins results in significant decreases in stiffness of supporting and hair cell apical surfaces and stereocilia bundles. (*A*) Topography and stiffness maps of the organ of Corti explants for wild-type *Triobp*$^{+/+}$, heterozygous *Triobp*$^{\Delta Ex8/+}$, and homozygous *Triobp*$^{\Delta Ex8/\Delta Ex8}$ mice. The schematic illustrates the locations of the apical surfaces of supporting cells phalangeal process and the hair cells cuticular plate within the reticular lamina. (*B*) E values for apical processes of IPCs, OPCs, DCs row 1 (DCs1), and DCs row 2 (DCs2) of *Triobp*$^{+/+}$, *Triobp*$^{\Delta Ex8/+}$, and *Triobp*$^{\Delta Ex8/\Delta Ex8}$, respectively. (*C*) E values for cuticular plates of three rows of OHCs including OHCs1, OHCs2 and OHCs3 of *Triobp*$^{+/+}$, *Triobp*$^{\Delta Ex8/+}$ and *Triobp*$^{\Delta Ex8/\Delta Ex8}$, respectively. The E values of the reticular lamina were measured in regions of interest (white square box in *Triobp*$^{+/+}$ Young's modulus image) overlaying the apical surface of supporting and hair cells. (*D*) Effective pivotal stereocilia stiffness values within hair bundles of three rows of OHCs. Note that *Triobp*$^{+/+}$ wild-type control results are the same for Figs. 4 and 5 since both mice strains used in this study are on the same C57BL/6 background. Data are represented as mean (kilopascals or piconewtons per nanometer) ± SD. Significant differences between conditions by unpaired two-tailed Student's *t* test with Welch's correction indicated as ****$P < 0.0001$, ***$P < 0.001$, **$P < 0.01$, and *$P < 0.05$. (Scale bars: 5 µm.) *SI Appendix*, Table S2 includes detailed statistical analysis.

"radial direction" is an orientation perpendicular to the longitudinal base to apex direction of the organ of Corti (Fig. 1*B*). PFT-AFM analyses allowed us to visualize the spatial changes in stiffness along the radial axis of live organ of Corti explants. The local stiffness of the reticular lamina at the apical surfaces of nonsensory supporting cells increases from PCs toward DCs. However, the local stiffness of the reticular lamina at the cuticular plates of sensory hair cells declines from the first toward the third row of OHCs. Thus, there are complex and bidirectional radial stiffness gradients in the organ of Corti reticular lamina consisting of oppositely oriented radial gradients for hair cells versus supporting cells (Fig. 7). This prompted us to hypothesize that supracellular epithelial tensional homeostasis (33) of the cochlear sensory tissue is achieved by balancing the mechanical properties between supporting cells and hair cells. However, our results show a more complex picture in which the sensory epithelium tissue stiffness is not balanced between sensory hair cell and neighboring supporting cells (Fig. 7*B*). In the wild-type mouse, the hair cell radial stiffness is the dominant gradient, which is more than 10-fold larger than for the supporting cell gradient (Fig. 7*B*).

Absence of Both TRIOBP-4 and TRIOBP-5 Diminishes Reticular Lamina Bidirectional Radial Stiffness Gradients. High-resolution PFT-AFM nanomechanical mapping was also utilized to monitor the radial stiffness gradient in the mouse organ of Corti reticular lamina of the wild-type *Triobp*$^{+/+}$, heterozygous, and homozygous mutant littermate mice. We first investigated the reticular lamina radial stiffness gradients behavior when only TRIOBP-5 was absent. For all genotypes (*Triobp*$^{+/+}$, *Triobp*$^{\Delta Ex9\text{-}10/+}$, and *Triobp*$^{\Delta Ex9\text{-}10/\Delta Ex9\text{-}10}$), the local stiffness of the reticular lamina at the apical surfaces of supporting cells increases from the PCs

toward the DCs (positive gradient). However, the magnitude of the radial stiffness gradient of supporting cell apical surfaces was reduced in the *Triobp* mutants compared with the wild-type *Triobp*$^{+/+}$ mouse (Fig. 7*B* and *SI Appendix*, Table S3). Furthermore, for all conditions, the local stiffness at the cuticular plates of sensory hair cells decreases from the first toward the third row of OHCs showing a negative gradient. Similarly, the magnitude of the radial stiffness gradient of the hair cell cuticular plates was significantly reduced ($P < 0.01$) as compared to the *Triobp*$^{+/+}$ mouse (Fig. 7*B* and *SI Appendix*, Table S3). Therefore, the absence of TRIOBP-5 reduces the reticular lamina radial stiffness gradients, although these stiffness gradients are not completely abolished.

Similar to *Triobp-5*-only–deficient mice, in the case of both TRIOBP-4 and TRIOBP-5 deficiencies (*Triobp*$^{+/+}$, *Triobp*$^{\Delta Ex8/+}$, and *Triobp*$^{\Delta Ex8/\Delta Ex8}$ mice) the local stiffness of the reticular lamina at the apical surfaces of supporting cells increases from the PCs toward the DCs (positive gradient). In addition, the radial stiffness gradient magnitude of supporting cell apical surfaces was significantly reduced in the *Triobp*$^{\Delta Ex8/+}$ and *Triobp*$^{\Delta Ex8/\Delta Ex8}$ mutants compared with wild-type *Triobp*$^{+/+}$ (Fig. 7*B* and *SI Appendix*, Table S3). Interestingly, in heterozygous *Triobp*$^{\Delta Ex8/+}$ mice, the magnitude of the radial stiffness gradient of the OHC cuticular plates is reduced but maintains its orientation similar to that of wild-type *Triobp*$^{+/+}$, while in homozygous *Triobp*$^{\Delta ex8/\Delta ex8}$ mice the gradient orientation was reversed (Fig. 7*B* and *SI Appendix*, Table S3). Altogether, absence of TRIOBP-4 and TRIOBP-5 or TRIOBP-5 alone significantly reduces the magnitudes of the reticular lamina radial stiffness gradient of supporting and OHCs, whereas the absence of both TRIOBP isoforms significantly alters the normal behavior (magnitude and orientation) of the radial stiffness gradient of hair cells. Therefore, both TRIOBP-4 and TRIOBP-5 are individually critical for the maintenance of optimal tissue-level reticular lamina radial stiffness gradients and their absence compromises the cochlear mechanical properties, which in turn may contribute to the pathophysiology of TRIOBP-deficient mice and the phenotype of human DFNB28 deafness.

Discussion

Mechanical interactions among neighboring OHCs of the organ of Corti depend on intricate relationships with the adjacent mosaic of supporting cells (PCs, OPCs, and DCs), which collaborate to form the reticular lamina (34–36) (Fig. 7*C*). No previous study has mapped the cochlear reticular lamina at nanoscale resolution due to the intrinsic low spatial resolution of previous biophysical approaches using glass micropipettes (23, 24), fluid jets (25), or standard AFM methods (26). In this study, using a nanoscale resolution PFT-AFM method, we measured the mechanical properties of the spatially heterogeneous apical surface of the cochlear sensorial reticular lamina, including individual hair cells and apical surfaces supporting cells, and revealed previously unknown radial gradients of stiffness with opposite orientations when supporting cell local stiffnesses are compared with hair cells.

Using two *Triobp* deaf mouse models that recapitulate human recessively inherited deafness DFNB28 (9, 10), we demonstrated essential roles in mechanical homeostasis of the F-actin–associated TRIOBP-4 and TRIOBP-5 proteins in inner ear tissue. Our findings indicate that the absence of both *Triobp* isoforms significantly reduces the stiffness of supporting cell apical surfaces, hair cell cuticular plates, and stereociliary bundles. Furthermore, our data also show the existence of cochlear reticular lamina composite radial stiffness gradients, which decrease from the first toward the third row of OHCs in the cuticular plates of the hair cells and increase from the second row of DCs to the IPCs in the apical surfaces of the supporting cells. These radial gradient magnitudes of stiffness are significantly diminished in *Triobp* mutant mice with greater reductions observed when TRIOBP-4 and TRIOBP-5 proteins are both absent as compared to loss of TRIOBP-5 only.

Microtubules and bundled actin filaments together are essential for the mechanical properties of the apical surfaces of sensory hair cells and supporting cells (37). This interplay was studied using molecular mediators such as latrunculin A, jasplakinolide, blebbistatin, taxol, and nocodazole (27). Here, our observations argue for the importance of the F-actin–binding proteins TRIOBP-4 and TRIOBP-5 for the characteristic mechanical properties of the cytoskeletal components of hair cells and supporting cells and for their overall apical surface stiffness. Recently, GAS2 (growth-arrest-specific 2), a protein with microtubule and F-actin–binding domains, was shown to be expressed in pillar and DCs colocalizing specifically with microtubules. Absence of GAS2 significantly reduced the stiffness of the supporting cell phalangeal processes (37). These observations raise additional questions as to the individual functions of other cytoskeleton-associated proteins of hair cells and supporting cells such as tropomyosin, spectrin, β-actin, γ-actin, espin, prestin, and tubulin and the effects of pathogenic variants in the corresponding genes on the cellular structures that might also contribute to the radial stiffness gradients we report here.

A longitudinal gradient along the length of the cochlear reticular lamina has been reported for frequency detection of sound, for hair cell and supporting cell morphology (3), and for the stiffness of organ of Corti individual sensory cells (38). For example, the relative stiffness of pillar cells is greater in the basal region of the cochlea where high-frequency sound is detected, while stiffness decreases toward the apex of the cochlea where low-frequency sound is detected. These surface mechanical properties of sensory and nonsensory cells have been attributed to changes in the cytoskeletal architecture (27). In addition, a longitudinal gradient in the length of stereocilia and the OHC bodies increases from base to apex (38). Interestingly, previous studies have also shown longitudinal and radial gradients of compositional, structural, and mechanical properties in the basilar membrane and in the acellular tectorial membrane that covers organ of Corti hair cells (39, 40). The overall structure and collagen fibril orientation and thickness of the tectorial membrane varies along the cochlea, which are hypothesized to underlie a decreasing basal-to-apical gradient in tectorial membrane stiffness in the region overlying hair cell stereocilia (39). The evidence for and implications of a longitudinal gradient along the cochlea (41) and a radial gradient (42) in tectorial membrane elasticity were reported and associated with a radial gradient in collagen fibril density (42, 43). In addition, different mechanical properties of the basilar membrane, such as its increasing stiffness toward the base, are graded along the length of the cochlea (40), although the factors that lead to the gradient in its mechanical properties are still unclear. Since longitudinal and radial gradients in mechanical properties have been previously shown in the tectorial and basilar membranes, we hypothesized that the organ of Corti reticular lamina may also possess a distinct and intricate radial gradient. We further hypothesize that existence of a radial stiffness gradient in the reticular lamina could help maintain the organ of Corti intricate sensitivity and frequency discrimination by providing a passive cochlear mechanical filtering that defines which OHC would enhance the auditory vibration

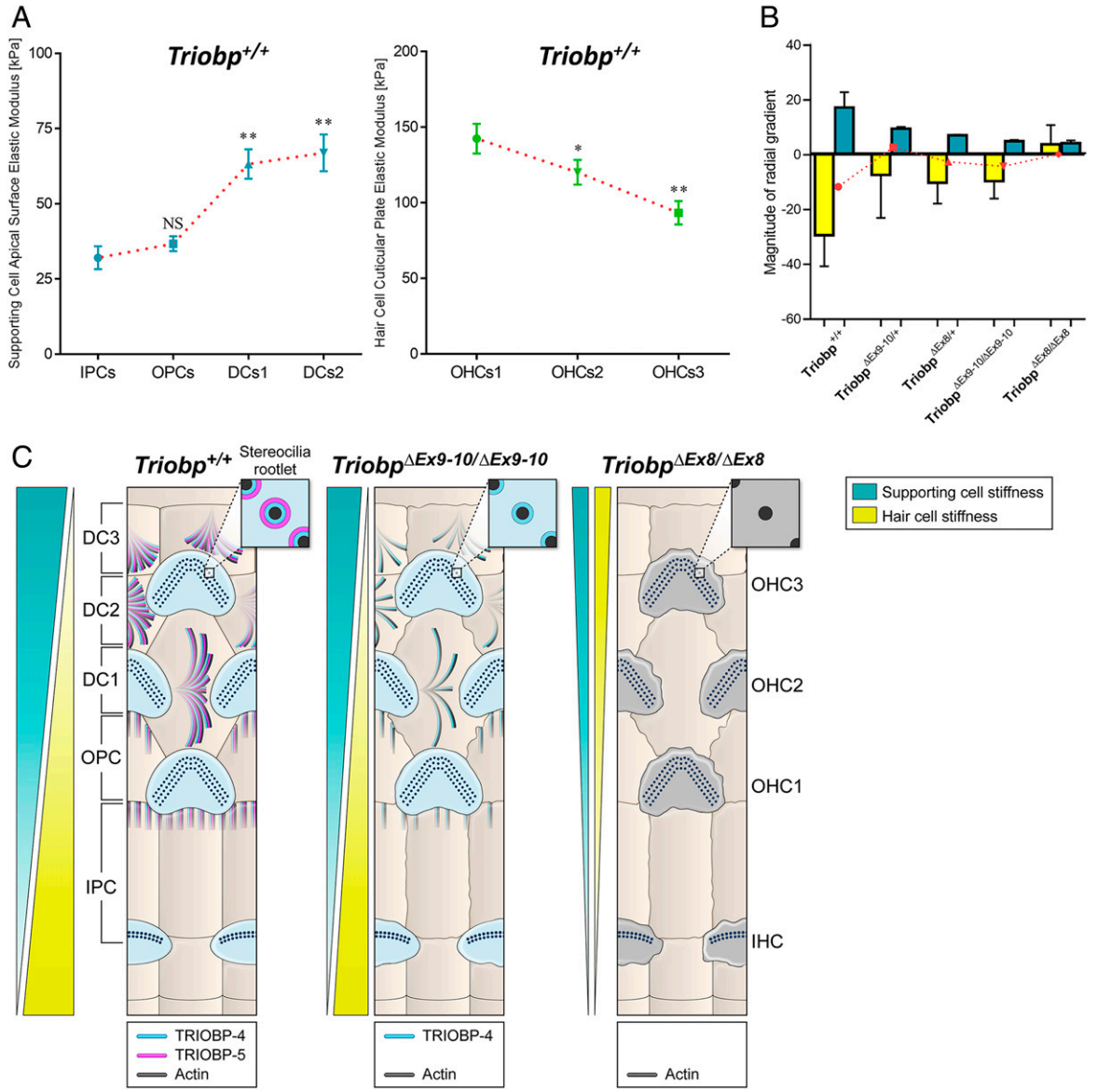

Fig. 7. Novel bidirectional radial stiffness gradients within the organ of Corti are promoted by TRIOBP expression. (*A*) Graphs show changes in measured Young's modulus of supporting cells (cyan) and OHCs (green) within the reticular lamina of P5-P6 wild-type mice. Data are represented as means ± SEM; NS indicates nonsignificant differences, $P > 0.05$ (by unpaired two-tailed Student's *t* test with Welch's correction); $^{**}P < 0.01$ and $^{*}P < 0.05$ indicates significant differences by unpaired two-tailed Student's *t* test with Welch's correction). *SI Appendix*, Tables S1 and S2 includes detailed statistical analysis. (*B*) Average slope magnitudes of radial gradients in Young's modulus values against cell position within the reticular lamina (slope; E/radial position) of supporting and hair cells for *Triobp*$^{+/+}$, heterozygous *Triobp*$^{\Delta Ex9\text{-}10/+}$, and homozygous *Triobp*$^{\Delta Ex9\text{-}10/\Delta Ex9\text{-}10}$ mice as well as heterozygous *Triobp*$^{\Delta Ex8/+}$ and homozygous *Triobp*$^{\Delta Ex8/\Delta Ex8}$ mice. Note that when TRIOBP-4 and TRIOBP-5 isoforms are both absent the reticular lamina radial stiffness gradients become unidirectional. The superimposed plot in red represents the comparison between supporting cells and hair cells for each condition indicating the residual stiffness between sensorial and nonsensorial cells. Data are represented as mean ± SEM. *SI Appendix*, Table S3 includes detailed statistical analysis. (*C*) Summary model describing opposing radial stiffness gradients in the reticular lamina of the organ of Corti. The illustration of TRIOBP-4 and TRIOBP-5 distribution in the stereocilia bundles, cuticular plate of hair cells and apical processes of supporting cells of wild-type (*Triobp*$^{+/+}$), *Triobp*$^{\Delta Ex9\text{-}10/\Delta Ex9\text{-}10}$ homozygous deficient for TRIOBP-5, and *Triobp*$^{\Delta Ex8/\Delta Ex8}$ homozygous deficient for both TRIOBP-4 and TRIOBP-5 (TRIOBP-4/5) and additionally demonstrating radial stiffness gradients in the organ of Corti reticular lamina of each one.

stimuli of particular frequencies. Our study demonstrates a complex radial mechanical stiffness gradient in the organ of Corti reticular lamina.

The organ of Corti mechanical properties regulate cochlear amplification (44, 45). Specifically, two mechanical conditions are responsible for location-dependent amplification of sound of high to low frequencies from base to apex of the cochlea. First, the phase of the OHC somatic electromotility force varies along the cochlear length. Second, the local stiffness of the organ of Corti varies along the cochlear length. However, the mechanisms for similar gradients in the radial direction of the organ of Corti remain unclear, although a radial morphology and gene expression asymmetries in the organ of Corti have been shown previously in the sensory hair cells of both adult and developing tissues (34). For instance, there are prominent longitudinal and radial gradients of the expression of prestin, a motor protein in the lateral wall of OHCs responsible for electromotility (46). Prestin immunostaining intensity increases in outer cells from base to apex and from the first to the third row of OHCs (47).

The possibility of a radial gradient in the mechanical properties of the organ of Corti is supported by computational simulations (48) and in vivo imaging (49). Sasmal and Grosh developed a mathematical model showing that the reticular lamina may indeed have radial passive and active mechanical properties (48). Radial

tuning in the reticular lamina of the mouse organ of Corti has also been reported by in vivo volumetric optical coherence tomography vibrometry measurements (49). Interestingly, this radial tuning of the reticular lamina is detected in a dead cochlea, when OHC no longer produce prestin-driven amplification of the electromotility force, and in the detached tectorial membrane mutants of TECTA, suggesting that the radial tuning of the reticular lamina is derived mainly from passive mechanical properties, including apical surface passive tension, stiffness, and viscosity, consistent with our discovered radial gradients in the measured passive mechanical property (Young's modulus). Additionally, radial tuning (passive mechanical properties) of the reticular lamina is not imparted, controlled, or modified by the tectorial membrane, justifying our preparations for measuring the apical stiffness of organ of Corti explants. Khanna and Hao conducted experiments on the apical turn of living guinea pig cochleae and reported a significant increase in detected vibration amplitude and phase shift in the radial direction of hair cells from IHCs toward the third row of OHCs (50), suggesting a softening of hair cells in the radial direction, consistent with our measurements. They also reported a significantly larger magnitude of detected amplitude of Hensen's cells compared to that of the hair cells, suggesting that supporting cells are significantly softer when compared to hair cells, an observation that is also consistent with our measurements.

The previously unreported bidirectional radial stiffness gradients discovered in this study provide experimental evidence of reticular lamina mechanical coordination to maximize hair bundle deflection, thus improving hearing sensitivity, frequency selectivity, and amplification. Any radial change in stiffness is significant because it would allow the OHCs from the first toward the third row to absorb high-frequency energy. This behavior is similar to the base-to-apex cochlear partition's ability to absorb high-frequency energy changes in fluid pressure, which declines toward the apex (51). Interestingly, a bidirectional change in radial stiffness with hair cells and supporting cells having different stiffness behaviors suggest diverse mechanisms of sound frequency discrimination possibly allowing efficient force transmission and simple radial shear within the reticular laminar. In other words, these opposite radial stiffness gradients will amplify radial motions within the reticular lamina. Otherwise, the longer stereociliary bundles of the OHCs third row, which have a much lower rotational stiffness than shorter OHCs of the first row, would be less sensitive to low sounds (small vibrations). Future studies in mouse with conditionally ablated TRIOBP expression only in supporting cells are needed to test the hypothesis that the radial stiffness gradient and changes in local supporting cell stiffness that we observed in *Triobp* mutant mice are required for normal hearing.

Previously we showed that the presence of both TRIOBP-4 and TRIOBP-5 is necessary for stereocilia rootlet formation and architecture and that hair cells with stereocilia lacking rootlets will subsequently die, causing deafness (9, 10). Here we show that TRIOBP-4 and TRIOBP-5, but not TRIOBP-1, are localized to the apical processes of DCs and apical cuticular plates of OPCs and are important for maintaining radial stiffness of the organ of Corti sensory epithelium. In $Triobp^{\Delta Ex9\text{-}10/\Delta Ex9\text{-}10}$ mutant mice, the immunochemistry observations (although not quantitative) show no differences in the TRIOBP-1 or TRIOBP-4 immunoreactivity as compared to the wild-type controls, consistent with our mRNA expression data. The role of TRIOBP-1 that is localized in association with the internal and external sulcus cell junctions awaits further investigations.

In conclusion, from the variety of genetic, ultrastructural, immunocytochemical, and molecular biological data in this study in support of our AFM-based nanomechanical maps, we revealed previously unknown bidirectional radial stiffness gradients in the reticular lamina of the mouse cochlea. The magnitude and orientation of these radial gradients requires the expression of TRIOBP in hair cells and supporting cells. The loss of TRIOBP-4 and TRIOBP-5 compromises these radial stiffness gradients of opposite orientation. The mammalian inner ear sensory epithelium should not be considered just as a rigid tissue. We speculate that the additional complexity of its mechanical properties that we have identified in this study, in particular localized tissue mechanical variation, is essential to hearing frequency sensitivity and selectivity in which TRIOBP is an important contributor.

Materials and Methods

Mouse Models and Genotyping. Wild-type $Triobp^{+/+}$, heterozygous $Triobp^{\Delta Ex9\text{-}10/+}$, and homozygous $Triobp^{\Delta Ex9\text{-}10/\Delta Ex9\text{-}10}$ mice as well as heterozygous $Triobp^{\Delta Ex8/+}$ and homozygous $Triobp^{\Delta Ex8/\Delta Ex8}$ mice were generated and genotyped as described previously (9, 10). For detailed descriptions, see *SI Appendix, Supplementary Materials and Methods*.

In Situ Hybridization Using RNAscope Probes. In situ hybridizations were performed using RNAscope Multiplex Fluorescent V2 assay (Advanced Cell Diagnostics) with the following probes. For detailed descriptions of RNAscope probes used, sample preparation, and data collection, see *SI Appendix, Supplementary Materials and Methods*.

ddPCR. The expression of the *Triobp* alternative splice isoforms was quantified using a QX200 ddPCR System (Bio-Rad) according to the manufacturer's instructions. For detailed descriptions of ddPCR probes used, sample preparation, and data collection, see *SI Appendix, Supplementary Materials and Methods*.

Electron Tomography with FIB Serial Sectioning and SEM Imaging. Cochleae from wild-type ($Triobp^{+/+}$), heterozygous ($Triobp^{\Delta Ex9\text{-}10/+}$), and homozygous ($Triobp^{\Delta Ex9\text{-}10/\Delta Ex9\text{-}10}$) mice at P6 and P7 were used. FIB-SEM stacks were imaged using a FEI Helios 660 Nanolab system in "Slice and View" mode with a backscattered electron detector. For detailed descriptions of FIB-SEM sample preparation, data collection, and analysis of FIB-SEM stacks, see *SI Appendix, Supplementary Materials and Methods*.

Immunostaining. P8 and P20 wild-type $Triobp^{+/+}$ and homozygous $Triobp^{\Delta Ex9\text{-}10/\Delta Ex9\text{-}10}$ mice were used for immunostaining of the organ of Corti with anti-TARA antibody (Proteintech, 16124-1-AP) which was developed against an antigen corresponding to the C-terminal sequence of TRIOBP-5 identical to TRIOBP-1, as reported (29). We also used antibodies against TRIOBP-4/5 and against TRIOBP-5 as previously described (9, 10). For detailed descriptions of immunostaining sample preparation, and confocal imaging, see *SI Appendix, Supplementary Materials and Methods*.

Organ of Corti Explant Cultures. Wild-type $Triobp^{+/+}$, heterozygous $Triobp^{\Delta Ex9\text{-}10/+}$, and homozygous $Triobp^{\Delta Ex9\text{-}10/\Delta Ex9\text{-}10}$ mice as well as heterozygous $Triobp^{\Delta Ex8/+}$ and homozygous $Triobp^{\Delta Ex8/\Delta Ex8}$ mice were used for explant culture experiments. Three P6 pups of each genotype were sacrificed by decapitation according to the National Institutes of Health Guidelines for Care and Use of Laboratory Animals. For detailed descriptions of cochlear sample preparation, see *SI Appendix, Supplementary Materials and Methods*.

PFT-AFM Imaging. PFT-AFM images were obtained using a Bruker BioScope Catalyst AFM system (Bruker) mounted on an inverted Zeiss Axiovert 200M optical microscope equipped with a 40× objective (0.95 numerical aperture, Plan-Apochromat, Zeiss) and a confocal laser scanning microscope (LSM 510 META, Zeiss). For detailed descriptions of the PFT-AFM nanomechanical mapping, generation and analysis of Young's modulus maps, and analysis of the pivotal stiffness of stereocilia, see *SI Appendix, Supplementary Materials and Methods*.

Statistical Analysis. All experiments were repeated at least three times. Data in Figs. 5 and 6 are shown in box-and-whisker plots. Bars show mean ± SD. Data in Fig. 7 are shown as mean ± SEM. Student's *t* tests of independent

variables (two-tailed *t* test with Welch's correction) were used to determine statistical significance and the asterisks indicate the level of statistical significance (*$P < 0.05$, **$P < 0.01$, ***$P < 0.001$, and ****$P < 0.0001$).

Study Approval. The experiments on mice were conducted according to the National Institutes of Health Guidelines for Care and Use of Laboratory Animals. All experimental procedures were approved by the National Institute of Neurological Disorders and Stroke/National Institute on Deafness and Other Communication Disorders Animal Care and Use Committee at the NIH (protocol 1263-20 to T.B.F.).

Data Availability. All study data are included in the article and/or *SI Appendix*.

ACKNOWLEDGMENTS. We thank Mr. Alan Hoofring (NIH's Medical Arts Design Section) for help with Illustrations in Figs. 1 and 7 and Ms. Sherly Michel (National Institute on Deafness and Other Communication Disorders [NIDCD]) and Mr. Pat Diers (NIDCD) for animal care and genotyping and Drs. Kuni Iwasa (NIDCD) and Benjamin Perrin (Indiana University–Purdue University Indianapolis) for reading the manuscript and providing critical inputs. A.X.C.-R. and this work was supported by the NIH Distinguished Scholars Program and the NIH Intramural Research Program of the National Institute of Biomedical Imaging and Bioengineering (grant 1ZIAEB000094). This research was supported (in part) by the Intramural Research Program of the NIH, NIDCD DC000039 to T.B.F. S.K. was supported by Japan Society for the Promotion of Science KAKENHI grant 20K09687 and G.I.F. by NIDCD/NIH (R01DC014658 and S10OD025130). The electron microscopy was performed at the University of Kentucky Electron Microscopy Center, which belongs to the NSF NNCI Kentucky Multiscale Manufacturing and Nano Integration Node, supported by ECCS-1542174.

Author affiliations: [a]Section on Mechanobiology, National Institute of Biomedical Imaging and Bioengineering, National Institutes of Health, Bethesda, MD 20892; [b]Laboratory of Molecular Genetics, National Institute on Deafness and Other Communication Disorders, National Institutes of Health, Bethesda, MD 20892; [c]Department of Physiology, University of Kentucky, Lexington, KY 40536; and [d]Department of Otolaryngology-Head and Neck Surgery, Kyoto University Graduate School of Medicine, Kyoto 606-8303, Japan

1. M. Anniko, Cytodifferentiation of cochlear hair cells. *Am. J. Otolaryngol.* **4**, 375–388 (1983).
2. L. Robles, M. A. Ruggero, Mechanics of the mammalian cochlea. *Physiol. Rev.* **81**, 1305–1352 (2001).
3. R. S. Kimura, The ultrastructure of the organ of Corti. *Int. Rev. Cytol.* **42**, 173–222 (1975).
4. A. M. Breglio *et al.*, Exosomes mediate sensory hair cell protection in the inner ear. *J. Clin. Invest.* **130**, 2657–2672 (2020).
5. J. McGrath, P. Roy, B. J. Perrin, Stereocilia morphogenesis and maintenance through regulation of actin stability. *Semin. Cell Dev. Biol.* **65**, 88–95 (2017).
6. P. Hakizimana, W. E. Brownell, S. Jacob, A. Fridberger, Sound-induced length changes in outer hair cell stereocilia. *Nat. Commun.* **3**, 1094 (2012).
7. D. N. Furness, S. Mahendrasingam, M. Ohashi, R. Fettiplace, C. M. Hackney, The dimensions and composition of stereociliary rootlets in mammalian cochlear hair cells: Comparison between high- and low-frequency cells and evidence for a connection to the lateral membrane. *J. Neurosci.* **28**, 6342–6353 (2008).
8. K. D. Karavitaki, D. P. Corey, Sliding adhesion confers coherent motion to hair cell stereocilia and parallel gating to transduction channels. *J. Neurosci.* **30**, 9051–9063 (2010).
9. S. Kitajiri *et al.*, Actin-bundling protein TRIOBP forms resilient rootlets of hair cell stereocilia essential for hearing. *Cell* **141**, 786–798 (2010).
10. T. Katsuno *et al.*, TRIOBP-5 sculpts stereocilia rootlets and stiffens supporting cells enabling hearing. *JCI Insight* **4**, e128561 (2019).
11. J. Bao *et al.*, R1 motif is the major actin-binding domain of TRIOBP-4. *Biochemistry* **52**, 5256–5264 (2013).
12. K. Seipel, S. P. O'Brien, E. Iannotti, Q. G. Medley, M. Streuli, Tara, a novel F-actin binding protein, associates with the Trio guanine nucleotide exchange factor and regulates actin cytoskeletal organization. *J. Cell Sci.* **114**, 389–399 (2001).
13. N. J. Bradshaw *et al.*, An unpredicted aggregation-critical region of the actin-polymerizing protein TRIOBP-1/Tara, determined by elucidation of its domain structure. *J. Biol. Chem.* **292**, 9583–9598 (2017).
14. T. Yano *et al.*, Tara up-regulates E-cadherin transcription by binding to the Trio RhoGEF and inhibiting Rac signaling. *J. Cell Biol.* **193**, 319–332 (2011).
15. Y. Zhu *et al.*, Phosphorylation of Tara by Plk1 is essential for faithful chromosome segregation in mitosis. *Exp. Cell Res.* **318**, 2344–2352 (2012).
16. S. Riazuddin *et al.*, Mutations in TRIOBP, which encodes a putative cytoskeletal-organizing protein, are associated with nonsyndromic recessive deafness. *Am. J. Hum. Genet.* **78**, 137–143 (2006).
17. H. Shahin *et al.*, Mutations in a novel isoform of TRIOBP that encodes a filamentous-actin binding protein are responsible for DFNB28 recessive nonsyndromic hearing loss. *Am. J. Hum. Genet.* **78**, 144–152 (2006).
18. T. J. Hoffmann *et al.*, A large genome-wide association study of age-related hearing impairment using electronic health records. *PLoS Genet.* **12**, e1006371 (2016).
19. A. Pollak *et al.*, Whole exome sequencing identifies TRIOBP pathogenic variants as a cause of post-lingual bilateral moderate-to-severe sensorineural hearing loss. *BMC Med. Genet.* **18**, 142 (2017).
20. M. Wesdorp *et al.*, Broadening the phenotype of DFNB28: Mutations in TRIOBP are associated with moderate, stable hereditary hearing impairment. *Hear. Res.* **347**, 56–62 (2017).
21. S. Park *et al.*, Emerging roles of TRIO and F-actin-binding protein in human diseases. *Cell Commun. Signal.* **16**, 29 (2018).
22. I. Pacentine, P. Chatterjee, P. G. Barr-Gillespie, Stereocilia rootlets: Actin-based structures that are essential for structural stability of the hair bundle. *Int. J. Mol. Sci.* **21**, 324 (2020).
23. R. C. Naidu, D. C. Mountain, Measurements of the stiffness map challenge a basic tenet of cochlear theories. *Hear. Res.* **124**, 124–131 (1998).
24. D. Strelioff, A. Flock, Stiffness of sensory-cell hair bundles in the isolated guinea pig cochlea. *Hear. Res.* **15**, 19–28 (1984).
25. M. Tobin, A. Chaiyasitdhi, V. Michel, N. Michalski, P. Martin, Stiffness and tension gradients of the hair cell's tip-link complex in the mammalian cochlea. *eLife* **8**, e43473 (2019).
26. A. X. Cartagena-Rivera, S. Le Gal, K. Richards, E. Verpy, R. S. Chadwick, Cochlear outer hair cell horizontal top connectors mediate mature stereocilia bundle mechanics. *Sci. Adv.* **5**, eaat9934 (2019).
27. K. B. Szarama, N. Gavara, R. S. Petralia, M. W. Kelley, R. S. Chadwick, Cytoskeletal changes in actin and microtubules underlie the developing surface mechanical properties of sensory and supporting cells in the mouse cochlea. *Development* **139**, 2187–2197 (2012).
28. J. K. Choong *et al.*, Nanomechanical mapping reveals localized stiffening of the basilar membrane after cochlear implantation. *Hear. Res.* **385**, 107846 (2020).
29. J. F. Krey *et al.*, ANKRD24 organizes TRIOBP to reinforce stereocilia insertion points. *J. Cell Biol.* **221**, e202109134 (2022).
30. P. Dallos, Outer hair cells: The inside story. *Ann. Otol. Rhinol. Laryngol. Suppl.* **168**, 16–22 (1997).
31. T. Ren, W. He, D. Kemp, Reticular lamina and basilar membrane vibrations in living mouse cochleae. *Proc. Natl. Acad. Sci. U.S.A.* **113**, 9910–9915 (2016).
32. A. J. Ricci, B. Kachar, J. Gale, S. M. Van Netten, Mechano-electrical transduction: New insights into old ideas. *J. Membr. Biol.* **209**, 71–88 (2006).
33. A. X. Cartagena-Rivera, C. M. Van Itallie, J. M. Anderson, R. S. Chadwick, Apical surface supracellular mechanical properties in polarized epithelium using noninvasive acoustic force spectroscopy. *Nat. Commun.* **8**, 1030 (2017).
34. G. Wan, G. Corfas, J. S. Stone, Inner ear supporting cells: Rethinking the silent majority. *Semin. Cell Dev. Biol.* **24**, 448–459 (2013).
35. E. V. Leonova, Y. Raphael, Organization of cell junctions and cytoskeleton in the reticular lamina in normal and ototoxically damaged organ of Corti. *Hear. Res.* **113**, 14–28 (1997).
36. R. L. Gulley, T. S. Reese, Intercellular junctions in the reticular lamina of the organ of Corti. *J. Neurocytol.* **5**, 479–507 (1976).
37. T. Chen *et al.*, Cochlear supporting cells require GAS2 for cytoskeletal architecture and hearing. *Dev. Cell* **56**, 1526–1540 (2021).
38. Z. F. Mann, M. W. Kelley, Development of tonotopy in the auditory periphery. *Hear. Res.* **276**, 2–15 (2011).
39. R. Gueta, E. Tal, Y. Silberberg, I. Rousso, The 3D structure of the tectorial membrane determined by second-harmonic imaging microscopy. *J. Struct. Biol.* **159**, 103–110 (2007).
40. G. Emadi, C. P. Richter, P. Dallos, Stiffness of the gerbil basilar membrane: Radial and longitudinal variations. *J. Neurophysiol.* **91**, 474–488 (2004).
41. C. P. Richter, G. Emadi, G. Getnick, A. Quesnel, P. Dallos, Tectorial membrane stiffness gradients. *Biophys. J.* **93**, 2265–2276 (2007).
42. S. P. Weaver, L. Schweitzer, A radial gradient of fibril density in the gerbil tectorial membrane. *Hear. Res.* **76**, 1–6 (1994).
43. B. Shoelson, E. K. Dimitriadis, H. Cai, B. Kachar, R. S. Chadwick, Evidence and implications of inhomogeneity in tectorial membrane elasticity. *Biophys. J.* **87**, 2768–2777 (2004).
44. Y. Liu, S. M. Gracewski, J. H. Nam, Two passive mechanical conditions modulate power generation by the outer hair cells. *PLOS Comput. Biol.* **13**, e1005701 (2017).
45. J. B. Dewey, B. E. Applegate, J. S. Oghalai, Amplification and suppression of traveling waves along the mouse organ of Corti: Evidence for spatial variation in the longitudinal coupling of outer hair cell-generated forces. *J. Neurosci.* **39**, 1805–1816 (2019).
46. P. Dallos, B. Fakler, Prestin, a new type of motor protein. *Nat. Rev. Mol. Cell Biol.* **3**, 104–111 (2002).
47. T. N. Judice *et al.*, Cochlear whole mount in situ hybridization: Identification of longitudinal and radial gradients. *Brain Res. Brain Res. Protoc.* **9**, 65–76 (2002).
48. A. Sasmal, K. Grosh, Unified cochlear model for low- and high-frequency mammalian hearing. *Proc. Natl. Acad. Sci. U.S.A.* **116**, 13983–13988 (2019).
49. H. Y. Lee *et al.*, Two-dimensional cochlear micromechanics measured in vivo demonstrate radial tuning within the mouse organ of Corti. *J. Neurosci.* **36**, 8160–8173 (2016).
50. S. M. Khanna, L. F. Hao, Reticular lamina vibrations in the apical turn of a living guinea pig cochlea. *Hear. Res.* **132**, 15–33 (1999).
51. C. R. Steele, J. G. Zais, Effect of coiling in a cochlear model. *J. Acoust. Soc. Am.* **77**, 1849–1852 (1985).